Microchimica Acta (2022) 189: 264
https://doi.org/10.1007/s00604-022-05359-6

ORIGINAL PAPER

Coupled electrochemiluminescent and resonance energy transfer determination of microRNA-141 using functionalized Mxene composite

Jin-Feng Du[1] · Jing-Shuai Chen[1] · Xing-Pei Liu[1] · Chang-Jie Mao[1] · Bao-Kang Jin[1]

Received: 15 January 2022 / Accepted: 25 May 2022 / Published online: 1 July 2022

Abstract

The electrochemiluminescence and resonance energy transfer (ECL-RET) method was adopted to detect miRNAs, in which the two-dimensional Ti_3C_2 Mxenes with high surface area modified with CdS:W nanocrystals (CdS:W NCs) were used as ECL signal emitter. Mxenes with a specific surface area of 5.2755 m^2/g carried more emitters and promote ECL intensity. As an energy acceptor, BiOCl nanosheets (BiOCl NSs) have a wide UV–Vis absorption peak in the range 250 nm–700 nm, including the emission band of CdS:W NCs with 520 nm emission wavelength. Hence, BiOCl NSs are covalently bound to hairpin DNA 2 by amide bond to quench the ECL signal of CdS:W NCs. In the presence of miRNA-141, the hairpin DNA 1 modified on the GCE was unfold and then paired with hairpin DNA 2 to release miRNA-141 and quench the signal of the ECL biosensor. Then, the concentration signal of miRNA-141 was amplified by catalytic hairpin assembly. The novel specific biosensor demonstrated a satisfactory linear relationship with miRNA-141 in the range 0.6 pM to 4000 pM; the detection limit was as low as 0.26 pM (3 s/m) under the potential of 0 ~ -1.3 V and showed outstanding RSD of 1.19%. The findings of the present work with high accuracy and sensitivity will be of positive significance for the clinical diagnosis of miRNA in the future work.

Keywords Electrochemiluminescence · Mxenes · ECL-RET · Circulation amplification

Introduction

MicroRNAs (miRNAs) are non-protein coding RNAs with short size and length of 18 to 24 nucleotides. Increasing studies have shown that single RNA can target several miRNAs and affect the expression of multiple genes [1]. As a result of regulating biological processes, miRNA is associated with many human cancers and played a crucial role in cancer expressing. Recently, the importance of miRNA detection was further proved by detecting miRNA in serum to distinguish cancer patients and healthy patients. Therefore, it is of great significance to establish a rapid and simple miRNA biosensor for the diagnosis of diseases [2]. In the early days, the miRNAs detection method depended on the strength of DNA hybridization, including north-ern blotting [3], microarrays [4] and so on. Nevertheless, the methods mentioned above may require expensive equipment and have other drawback of complex operation. Therefore, many electrochemical methods have been developed for detection due to their advantages of high stability, low background signal and simple operation. The development of electrochemical biosensor strategies for miRNAs has been widely used, which contains electrochemiluminescence (ECL) [5], photoelectrochemical (PEC) [6] and others. Designing a sensor with high sensitivity, low cost and simple run is of profound significance for miRNA detection.

Electrochemiluminescence and resonance energy transfer (ECL-RET) occur only when the ECL emission spectra of donor chromophore overlap with the UV- visible absorption spectra of receptor [7, 8]. Different from traditional electrochemiluminescence system, ECL-RET with higher sensitivity and lower background signal on account of resonance energy transfer from luminophor to quencher is observed.

✉ Xing-Pei Liu
414043594@qq.com

✉ Chang-Jie Mao
maochangjie@sina.com

[1] Key Laboratory of Structure and Functional Regulation of Hybrid Materials (Ministry of Education), School of Chemistry and Chemical Engineering, Anhui University, Hefei 230601, Anhui, China

ECL-RET shows effective characteristics in a variety of detection such as heavy mental ions, protein, small piece of DNA and medicine testing [9]. ECL-RET is also a classical detection method. By carrying its advantages in efficient and sensitive detection in ECL analysis technology, ECL-RET is still the approach of universal choice [10, 11]. As known, semiconductor nanocrystals with remarkable luminescence property and unique electronic characteristics, as well as its narrow emission band, controlled chemical surfaces, and undergo redox active with their co-reactants. These qualities brought it wider attention to the ECL donors. [8, 12, 13]. In view of the molecular relaxation exists in aqueous solution, the electron transfer rate slows down during the redox reaction process in most of emitter co-reactant H_2O_2 ECL system. To overcome this shortcoming, the reaction system needs more OH•, which was generated between the co-reactant H_2O_2 and the luminophor. Metal ions doping nanocrystals (NCs) provide a reliable way to solve this problem. Studies have demonstrated that metal ions doped NCs change the surface of NCs. As a general rule, this change can produce new electron energy level or obstruct the host energy level [8]. The receptor AuNPs/AgNPs is widely used in today's ECL-RET analysis; considering the cost of noble metals, non-noble metals acceptors have been expected to develop in ECL-RET system with wider UV–Vis absorption. Therefore, a novel biosensor was constructed from ECL donor CdS:W to acceptor BiOCl, which induce quenching of most emitters. Here, we design ECL-RET biosensor depended on BiOCl.

Nanomaterials are not only used as luminophor or ECL acceptor, but some metal nanomaterials also have catalytic effect on ECL emission in biosensor. The introduction of nanomaterial with catalytic properties can greatly enhance the performance of ECL biosensor [14]. Individual emitters are not convenient for electrochemical testing since the emitters are unstable in water; it is necessary to adopt a substrate material to fix more emitters. During the past decades, two-dimensional materials have become the most widely used materials in the field of sensors because of their large specific surface area, higher electron transfer rate, longer lasting stability and outstanding biocompatibility. For example, graphene has been well studied to building biosensors as a novel sensing platform [15]. Recently, Mxene appears in chemical research, it is a new family composed of more than 60 two-dimensional (2D) metal carbides, nitrides or carbonitrides. Due to its well energy storage capacity, Mxene has made great strides in wide varieties of electrochemical territories, including lithium-ion batteries, non-lithium-ion batterie, supercapacitors and so on [16]. And then, the A element of the MAX surface will be substituted by -F and -OH/=O to form the $M_{n+1}X_n$ (Tx) (where T denotes the terminal group -F and -OH/=O). The transition metal carbides have hydroxyl or oxygen terminated on their surfaces which not only endow Mxenes with better conductivity, but also improve the hydrophilicity of nanosheets [17]. Compared to other 2D materials, the surface functionalization of Ti_3C_2 Mxenes makes it not easy to aggregate and has electrochemical properties. In addition, metal ions can be inserted between layers of Ti_3C_2 Mxenes to develop better electrochemical capabilities. Using the outstanding properties discussed above, Ti_3C_2 Mxenes was selected to enhance the emission performance and load the emitter and has emerged as promising nanomaterials employed in electrochemiluminescence (ECL) [18, 19].

In this work, we established novel electrochemiluminescence sensors applied for the sensitive detection of microRNA-141. Ti_3C_2 Mxenes nanosheets (NSs) with high specific surface area can capture a great quantity CdS:W NCs by covalent bonding; the hydrophilic groups carried by the material are more friendly to the biosensor. The ECL response of biosensing platform is greatly enhanced. Combined with catalytic hairpin assembly process (CHA), BiOCl NSs have been used for the first time as quencher with excellent results, which causes miRNA-141 to be released into the next cycle, more hairpin DNA-BiOCl is fixed to the GCE, and then, the ECL intensity is remarkably quenched via the dissipation of non-radiative energy. Compared with other biosensor constructed for miRNA detection [20], the prepared ECL biosensor has wider linear range and sensitivity. In addition, the biosensor has greater potential in practical application with low-cost efficiency, strong selectivity to miRNA, simple operation and easy repetition make it have greater potential in practical application. This study provides a new strategy for the future development of miRNA detection.

Experiment

Materials and instrumentations

The details are displayed on Supplementary Information.

Synthesis of materials

The detailed process of material synthesis is shown in Supplementary Information.

Assembly of the biosensor

The fabrication process of the biosensor was illustrated in Scheme 1. Ten μL of Ti_3C_2 Mxenes/CdS:W NCs composites was dropped in the surface of polished GCE and dried. Subsequently, 10 μL 1.8 μM hydrosulfonyl-modified H1 (diluted with TE) was added to the modified GCE and incubated at 4℃ for 16 h. After rinsed with TE, 10 μL MCH (1 mM)

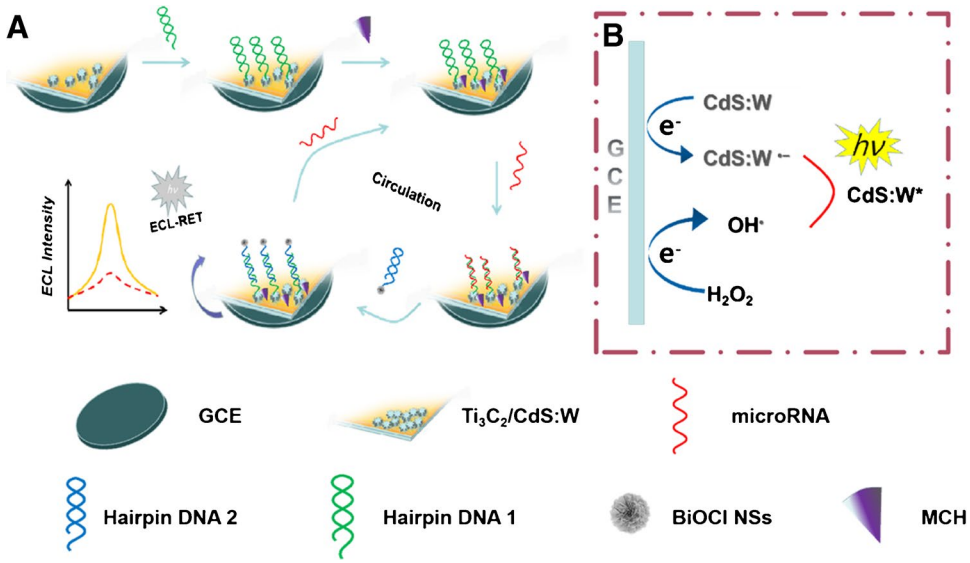

Scheme 1 The construction process of the biosensor BiOCl NSs@H2/miRNA/MCH/H1/Ti_3C_2 Mxenes/CdS:W NCs/GCE (**A**), electrochemiluminescence mechanism of emitters CdS:W NCs and co-reactants H_2O_2 (**B**)

diluted with PBS (PH = 7.4) was added to block the non-specific binding site, and then incubated at 37℃ for 30 min. The modified GCE was cleaned with PBS buffer to obtain H1/Ti_3C_2 Mxenes@CdS:W/GCE. In order to complete the detection process, 10 μL different concentrations of miRNA (diluted with DEPC buffer) and 10 μL H2-BiOCl-COOH NSs were employed on the GCE and incubated at 37℃ for 2 h, after rinsed with PBS buffer and stored at 4℃.

The final GCE was tested as follows: the biosensor was measured in the PBS (PH = 7.4) containing 75 mM H_2O_2. The scanning potential ranged of 0 to -1.3 V with a scanning rate of 100 mV/s. The PMT high voltage was 400 V.

Results and discussion

Characterizations of composites

The appearance of materials is shown in Fig. 1. The layered structure can be found in the SEM image of Ti_2C_3 Mxenes

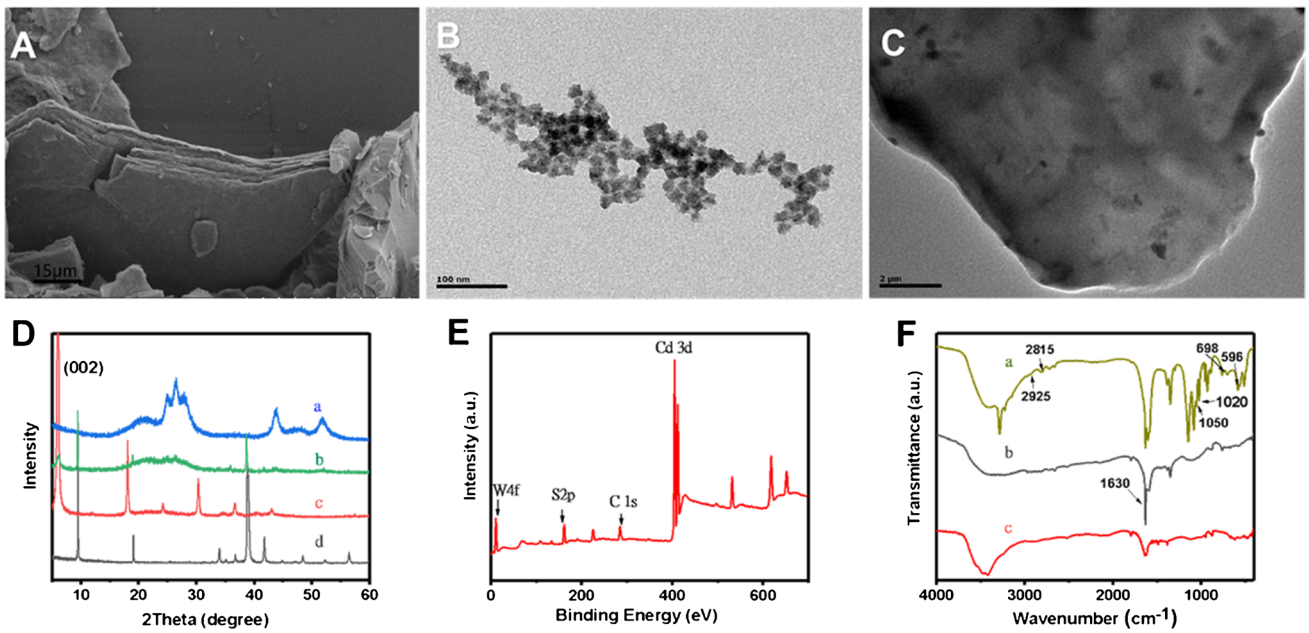

Fig. 1 SEM of Ti_2C_3 Mxenes NSs (**A**), TEM of CdS:W NCs (**B**) and TEM of composites (**C**), XRD patterns (**D**) of CdS:W NCs (a); CdS:W NCs/Ti_2C_3 Mxenes NSs (b); Ti_2C_3 Mxenes NSs (c); Ti_3AlC_2 MAX (d), XPS spectrum of CdS:W NCs (**E**). FT-IR spectra (**F**) of CdS:W NCs (a), Ti_2C_3 Mxenes NSs (b), CdS:W NCs/Ti_2C_3 Mxenes NSs (c)

nanosheets (Fig. 1A), indicating that Ti_3AlC_2 MAX was successfully stripping. The TEM image is displayed in Fig. 1B; the average size of snowflake CdS:W NCs is 20–30 nm. As demonstrated in X-ray photoelectron spectroscopy (XPS) of CdS:W NCs (Fig. 1E), the element peaks of Cd, S, W indicate that W element is successfully doped in CdS:W NCs. High resolution scans of C 1 s, S 2p, Cd 3d and W 4f are shown in Fig. S1. Subsequently, it can be seen from the TEM image in Fig. 1C that the CdS:W NCs is successfully loaded on the Ti_2C_3 Mxenes NSs.

In addition, compared with the XRD pattern of bulk MAX phases Ti_3AlC_2 (Fig. 1D, curve d), XRD pattern of Ti_2C_3 Mxenes NSs (Fig. 1D, curve c) displayed that the peak of $2\theta = 39°$ disappears and (002) peak shift to a lower angle. The difference figures out that Ti_2C_3 Mxenes NSs are prepared successfully by etching with HF [21]. At the same time, the XRD pattern of the composites is shown in curve b of Fig. 1D. The characteristic peak of Ti_2C_3 Mxenes NSs can be observed at 6° (002); the diffraction peak of 24.80°, 26.50°, 28.18°, 43.68°, 47.86° and 51.82° corresponds to crystallographic planes (100), (002), (101), (110), (103) and (112) of CdS NCs, which proved the existence of both in the composite according to the discovery of the above characteristic peaks.

The Fourier transform infrared spectroscopy (FT-IR) is assessed to the chemical bonds contained in the prepared material. As illustrated in Fig. 1F, curve a, Cd-S stretching vibration discovered at wavenumber 698 cm^{-1}. Besides, due to the doping of W element, the stretching vibration absorption peak of W-S bond is blue shifted and appears at 596 cm^{-1}. The peaks at 1050 cm^{-1} and 1020 cm^{-1} are attributed to hydroxyl group (-OH) on the surface of CdS:W nanocrystals [22, 23]. FT-IR spectra of Ti_2C_3 Mxenes NSs are shown in Fig. 1F, curve b. The strong absorption at 1630 cm^{-1} is the characteristic peak of N–H chemical bond, which belongs to the amino group ($-NH_2$) of PEI. Hence, the PEI is successfully modified onto the Ti_2C_3 Mxenes NSs. The wide absorption peak appeared at 3400 cm^{-1} (νO-H) is the external water on the surface of Ti_2C_3 Mxenes NSs [24].

Characterizations of BiOCl nanosheets (NSs)

The details are displayed on Supplementary Information.

Characterization of the electrochemistry and quenching mechanism about proposed biosensor

Electrochemical impedance spectrum (EIS) and ECL were employed to understand the step-by-step manufacturing process of the sensor. EIS (Fig. 2A) is a commonly method to assess the integrity of ECL biosensor assembly. The spectrum is divided into two parts. The semicircle part represents the resistance (Ret) and the straight portion represents the diffusion process in the low-frequency region [25]. In this experiment, the EIS detection was carried out in PBS (PH = 7.4, 0.01 M) containing 0.1 M KCl and 2 mM $[Fe(CN)_6]^{3-/4-}$. The resistance of bare GCE (curve a) is

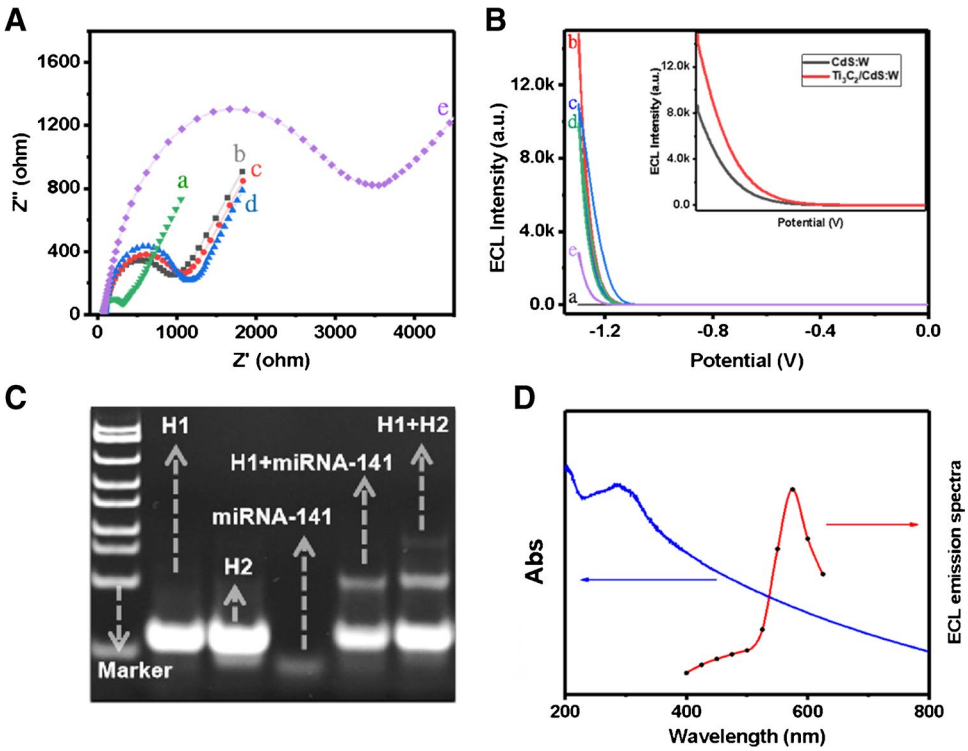

Fig. 2 EIS in PBS (PH = 7.4, 0.01 M) containing 0.1 M KCI and 2 mM $[Fe(CN)_6]^{3-/4-}$ (**A**) and ECL response potential in PBS (PH = 7.4, 0.01 M) containing 75 mM H_2O_2 (**B**) of bare GCE (curve a); Ti_3C_2 Mxenes/CdS:W/GCE (curve b); hairpin DNA 1/Ti_3C_2 Mxenes/CdS:W/GCE (curve c); MCH/hairpin DNA 1/Ti_3C_2 Mxenes/CdS:W/GCE (curve d); hairpin DNA 2-BiOCl/MCH/hairpin DNA 1/Ti_3C_2 Mxenes/CdS:W/GCE (curve e). PAGE to identify the occurrence of the proposed CHA (**C**), the concentration of each reactant species is 2 μM, and the reactions are performed at 37 °C for 2 h. Lane 1, marker; lane 2, H1; lane 3, H2; lane 4, miRNA; lane 5, H1 + miRNA; lane 6, H1 + miRNA + H2. The UV–Vis (**D**) of BiOCl NSs (curve blue); the ECL spectra of Ti_3C_2 Mxenes/CdS:W (curve red)

extremely smaller than that of the CdS:W/Ti_3C_2 (curve b). Hence, the material is successfully assembled on the electrode. Additionally, the Ret value is increased as the gradual modification of the electrode (Fig. 2A, curve b, c, d, e). The negative charge of H1 increased the electrostatic repulsion between GCE and electrolyte, making for an increase in Ret value [26]. Meanwhile, the resistance increases further when H2-BiOCl hybridizes with H1 and releases miRNA. The EIS diagram illustrated that the sensor is successfully assembled.

The cathodic CV and ECL of Ti_3C_2 Mxenes@CdS:W NCs/GCE in air free 0.10 M PBS and pH 7.4 containing different concentration of H_2O_2 are shown in Fig. S5-B. It can be concluded that H_2O_2 participates in CdS:W NCs luminescence as co-reactant. The ECL mechanism is shown in below:

$$H_2O_2 + e^- \rightarrow OH- + OH\bullet \quad (1)$$

$$CdS:W + e^- \rightarrow CdS:W\cdot- \quad (2)$$

$$2CdS:W\cdot- + 2OH\bullet \rightarrow CdS:W* + H_2O_2 \quad (3)$$

$$CdS:W* \rightarrow CdS:W + h\nu \quad (4)$$

Figure 2B shows the ECL intensity of varying degrees biosensor. In the PBS (0.1 M, PH = 7.4) buffer containing 75 mM H_2O_2, the bare electrode exhibits the lowest ECL intensity. After the CdS:W NCs (Fig. 2B) loaded onto glassy carbon electrodes, the ECL intensity increased significantly in the sweep range of -1.3 V to 0 V. At the same time, in consequence of larger surface area and better electroconductibility of Ti_2C_3 Mxenes NSs, the ECL response of the Ti_3C_2 Mxenes@CdS:W NCs (curve b) is significantly enhanced than that of CdS:W alone. Following hairpin DNA 1 (H1) bound to the material via Cd-S covalent bond. The obvious decrease of ECL intensity is attributed to the increase of resistance (curve c). After the non-specific sites were blocked by the addition of MCH, the ECL intensity was further decreased slightly (curve d). Finally, the ECL signal obviously reduced due to resonance energy transfer after the target miRNA-141 and BiOCl of the object to be measured were incubated in the sensor (curve e).

The crucial principles of CHA were summarized as following situation during the process. Firstly, the hairpin structure of DNA 1 was expanded by the target miRNA-141 on account of the bases complement each other. Secondly, the introduction of H2-BiOCl NSs triggered a series of amplification. Compared with H1•miRNA-141, the miRNA-141 were released behind H1 selectively bound to H2 in the reaction system, which could continue to open the hairpin of H1. The double-strand DNA H1•H2 is formed in the biosensor. In the end, the amount of miRNA-141 was amplified by CHA. Using catalytic hairpin assembly amplification to cause recycling of the miRNA of the object to be tested, the ECL response was effectively quenched after more H2-BiOCl binding to the sensor. Polyacrylamide gel electrophoresis (PAGE) (Fig. 2C) further demonstrated the cyclic relationship between hairpin DNA and miRNA in CHA amplification, the line 2, line 3 and line 4 bands correspond to H1, H2 and miRNA, respectively. The new bands observed in line 5 were assigned to H1•miRNA. After the CHA process, a band was produced by H2•H1 in line 6. Thus, it can be seen that the released miRNA continuously binds to H1 to open the repeat cycle. The above-obtained results show that ECL biosensor was successfully developed.

In order to confirm that there is resonance energy transfer between CdS:W NCs and BiOCl NSs. The UV–Vis absorption spectra of BiOCl NSs and ECL emission spectra of CdS:W NCs were obtained and shown in Fig. 2D, which has shown the wider UV–Vis absorption spectra of the receptor located at 520 nm, and have a good overlap with the electrochemical ECL spectrum of the emitter. It indicates the possibility of energy transfer.

Optimization of sensor construction conditions

A type of effective ECL performance has been closely related to experimental conditions. Optimizing the proportion of composite materials, concentration of the co-reactant H_2O_2, hairpin probe and the incubating time of miRNA need to be adapted. First, ECL intensity were measured by means of several Ti_3C_2/CdS:W in different proportions in Fig. 3A. Holding everything else constant, the optimal ECL response was achieved when the ratio of CTi_3C_2 to CCdS:W (mg/mL) was 0.5; with the excessive content of Ti_3C_2 in the materials, electron transfer is impeded and ECL decreases. As a result, Ti_3C_2@CdS:W with a ratio of 0.5 was prepared for sensor testing. As shown in Fig. 3B, the ECL intensity fluctuates slightly before the H_2O_2 concentration reaches 75 mM. After that, ECL intensity decreases as the concentration continues, which could put down to that excessive OH^- with the resulting $CdS:W^{\cdot-}$. The amount of hairpin probe 1 is related to the subsequent design of the sensor. Different ECL signals were monitored by dropping different concentrations of H1 into GCE, the receding ECL intensity with the concentration H1 up to 1.8 μM (Fig. 3C). Hence, 1.8 μM is the optimum concentration of H1. As shown in Fig. 3D, the cyclic amplification time of biosensor which was investigated includes 0.5 h to 2.5 h at 37℃; the lowest ECL was observed when incubation time reaches 2 h, in which the quenching effect is maximized about BiOCl. Finally, the optimization results under different conditions were shown in Fig. S6.

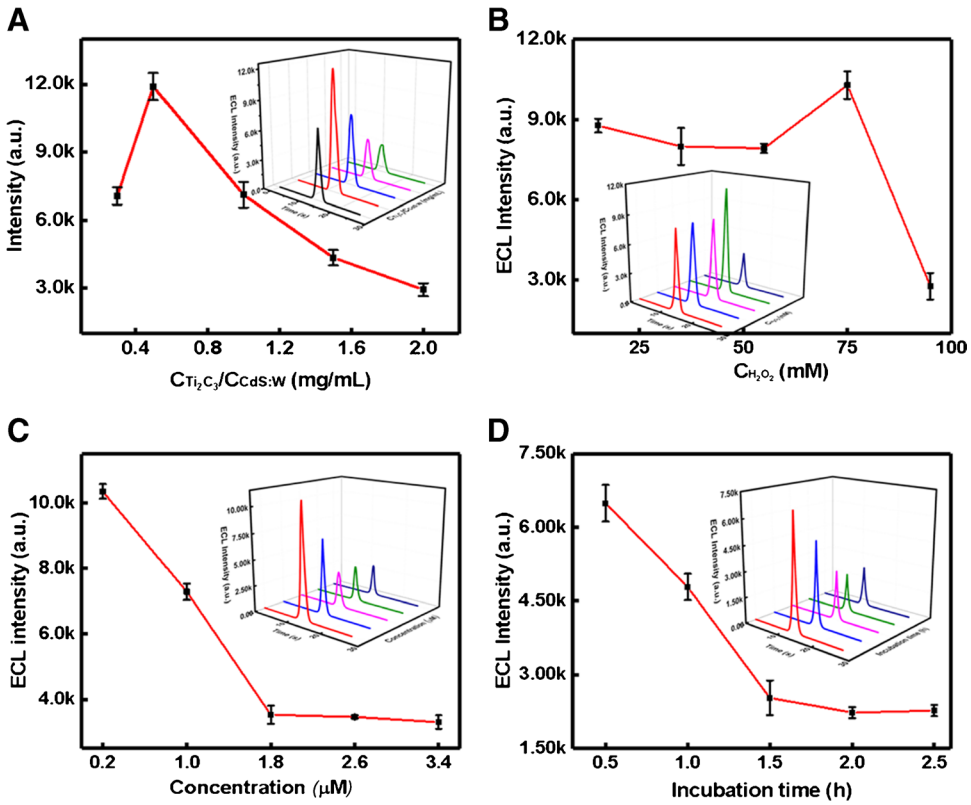

Fig. 3 Optimization of (**A**) the ratio of CTi_3C_2 to CCdS:W;(**B**) the concentration of H_2O_2 co-reactant; (**C**) the concentration of hairpin 1; (**D**) the incubation time of target miRNA

ECL biosensor for RNA detection

ECL measurement was implemented on the target miRNA-141 under optimized experimental conditions. Ten μL of miRNA-141 was dropped into the GCE for ECL analysis (Fig. 4A). The relationship between ECL intensity and the logarithm of miRNA concentration displayed a negative linear correlation in a range from 0.6 pM to 4000 pM. The linear equation was I = 12932.41–2958.87 logCmiRNA (unit of C was pM). The correlation coefficient was 0.998 and a detection limit achieved 0.26 pM (3 s/m). Compared with previous studies (Table 1), the established biosensor has lower detection limit at the concentration with wider dynamic detection range, and this approach proved to be of practical significance in reference to the reports of detecting the serum of real patient [27].

Reproducibility, stability, specificity of the sensor

As is well known, stability, reproducibility and specificity are the keys to evaluate the performance of ECL biosensor. ECL intensity stability was primarily examined under the optimized conditions. After 39 consecutive scanning cycles, there is an inconspicuous fluctuation in ECL intensity, and the relative standard deviation (RSD) is 1.19% (Fig. 4C). Hence, the stability of this biosensor is well. Otherwise, the blank sample, 1000 pM miRNA-155, miRNA-21, miRNAlet-10b, single-base mismatched miRNA (SM-miRNA), 1 nM Fe^{2+} and 1 μg/L aspirin (acetylsalicylic acid) were analyzed for the biosensor specificity (Fig. 4D, c → i). Compared with miRNA-141, the ECL intensity of blank sample and interference sample are not quenched, which indicate that the method is selective enough over chemically related organic species, or over chemically related drugs, or over chemically related ions. To understand that the recognition ability of the biosensor for mixed miRNA, we mixed miRNA-141 and miRNA-21 with the same amount of 4000 pM and then monitored their ECL response signals (Fig. 4D-a). The ECL intensity of mixture sample is similar to the single miRNA-141 sample (Fig. 4D-b). And as expected, the biosensor has strong recognition of miRNA-141. To reveal the stability of the biosensor, the sensor was preserved at 4℃ for one month, and then measured under the same conditions. As displayed in Figure S5-A, the luminescence intensity is reduced by less than 20% within the acceptable range, which shows the sensor still has excellent performance after long time storage.

MiRNA-141 were analyzed in spiked sample

In order to confirm the feasibility of ECL biosensor, the spiked samples were examined via standard addition method. The healthy human serum was diluted 10 times by PBS (0.1 M, PH = 7.4). One mL of 1 nM miRNA-141

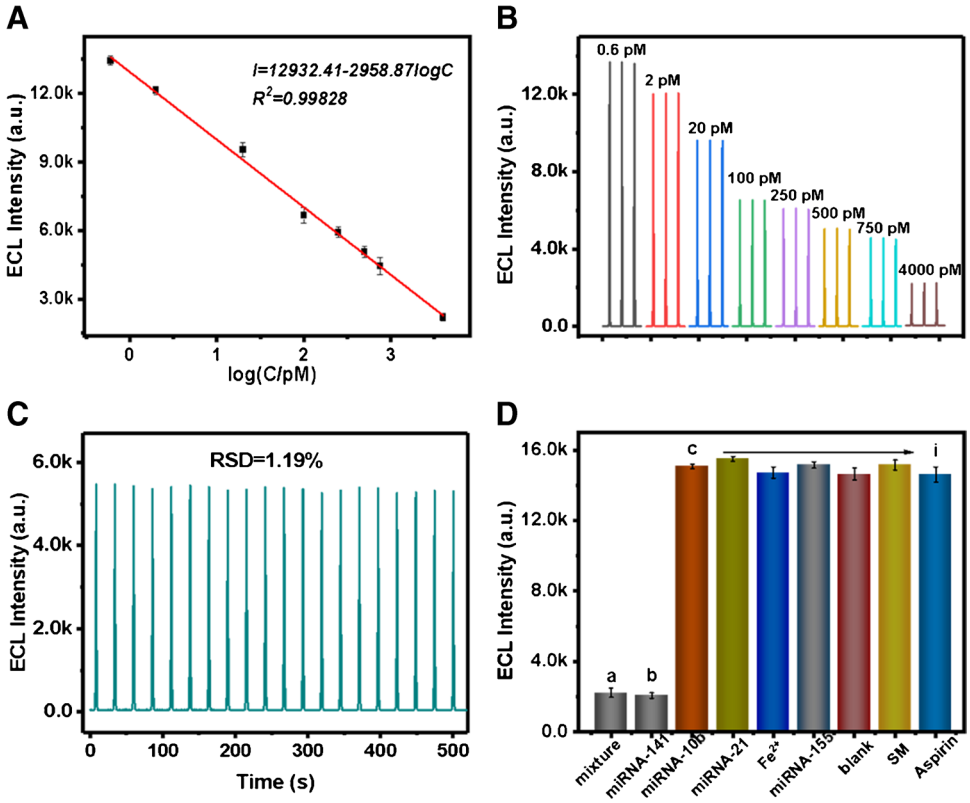

Fig. 4 The linear relationship between ECL intensity and the log CmiRNA: 0.6 pM, 2 pM, 20 pM, 100 pM, 250 pM, 500 pM, 750 pM, 4000 pM (**A**); ECL responses of the sensor with different concentrations of miRNA-141 in the range of 0.6 pM to 4000 pM (**B**); stability (**C**) and specificity (**D**) with different interfering substances miRNA let-10b, miRNA-21, Fe^{2+}, miRNA-155, blank, SM-miRNA, aspirin and mixture of ECL biosensor

Table 1 Comparison of this method with other methods reported in the literature

Material	Method	Target	Linear range (pM)	LOD (pM)	Refs
EXO III	MS	miRNA-141	$0–5\times10^3$	1.00	[28]
AgNCs/DHD	FL	miRNA-141	$0–1\times10^4$	6.10	[29]
Fe-MIL-88	AMI	miRNA-21	$10–2\times10^5$	13.00	[30]
Spinach	FL	miRNA	$10–1\times10^5$	3.00	[31]
Gold nanostripes	SPR	miRNA-125b	20–40	17.00	[32]
ZnSe-COOH/AuNFs	PEC	miRNA-122a	$0.35–7\times10^3$	0.16	[33]
CdS:WNCs/Ti_3C_2 Mxenes	ECL	miRNA-141	$0.6–4\times10^3$	0.26	This work

standard sample was taken and diluted to 5 pM, 50 pM, 500 pM with tenfold serum dilution. Then, three different concentrations of samples were measured under optimized conditions. The ECL response signal of the prepared sensor was detected under the scanning potential range of 0 to -1.3 V. The results are shown in Table 2. The recoveries are 105.95%, 96.02%, 92.00%, respectively, which are within the acceptable range calculated by linear regression equation. And the relative standard deviation (RSD) (n = 3) obtained by repeated tests is between 0 and 3.8%, which indicates that the biosensor has satisfactory precision. At the same time, a spiked mixture of 1000 pM miRNA-141 and 1000 pM miRNA-21 was added to human serum for ECL test displayed in Table 2. We got compelling recovery rate 106.98%, which proves that the biosensor has a promising application prospect not only for purified miRNA but also for mixed samples. The results showed that the designed sensor has advantage of being sensitive, stable and better recovery. But the detection limit (LOD) of this work is a

Table 2 Measurement of miRNA-141 in spiked sample

Serum sample	Added (pM)	Found (pM)	Recovery	RSD (%, n = 3)
1	0	0.092	0.00	1.65
2	5	5.30	105.95	3.79
3	50	48.01	96.02	2.23
4	500	459.456	92.00	2.59
5	1000 (mixture)	1069.84	106.98	3.72

direction where crucial improvements are needed, and further exploration in this field can be carried out in the future. Even so, it has been proved that the biosensor designed by us had a great potential for application after testing the spiking human serum samples.

Conclusion

A highly sensitive electrochemiluminescence biosensor was successfully constructed in this manuscript. Owing to larger specific surface area and excellent electrical conductivity, Ti_2C_3 Mxenes was compound with CdS:W to enhance its ECL performance. The application of Mxene in sensing field is also extended. BiOCl NSs with wider UV-via absorption were chosen as the resonance energy transfer acceptor for the first time. It has been proved that BiOCl NSs have strong quenching performance in biosensor. And it is turned out that the sensing platform based on ECL-RET effect exhibited excellent ECL response and low detection limit for miRNA-141. Most importantly, it is also an urgent searching nanomaterials with better performance for bioanalysis. This work provided a more original and efficient method for the detection of miRNA and explored a broader idea for the detection of biological molecules in the future.

Supplementary Information The online version contains supplementary material available at https://doi.org/10.1007/s00604-022-05359-6.

Acknowledgements This work was supported by National Natural Science Foundation of China (21976001). Natural Science Foundation of Anhui Province (1508085MB37). University Collaborative Innovation Project of Anhui Province (GXXT-2019-023). Natural Science Research Projects of Universities in Anhui Province (KJ2021A0030). Open fund for Discipline Construction of Institute of Physical Science and Information Technology.

Authors contribution **Jin-Feng Du** was involved in conceptualization, investigation, writing—original draft. **Jing-Shuai Chen** helped in methodology, investigation. **Xing-Pei Liu** contributed to validation. **Chang-Jie Mao** was involved in supervision, writing—review & editing. **Bao-Kang Jin** helped in writing—review & editing.

Declarations

Conflicts of interest There are no conflicts to declare.

References

1. Lu TX, Rothenberg ME (2018) MicroRNA. J Allergy Clin Immunol 141:1202–1207. https://doi.org/10.1016/j.jaci.2017.08.034
2. Tian T, Wang J, Zhou X (2015) A review: microRNA detection methods. Org Biomol Chem 13:2226–2238. https://doi.org/10.1039/C4OB02104E
3. Valoczi A, Hornyik C, Varga N, Burgyan J, Kauppinen S, Havelda Z (2004) Sensitive and specific detection of microRNAs by northern blot analysis using LNA-modified oligonucleotide probes. Nucleic Acids Res 32:e175. https://doi.org/10.1093/nar/gnh171
4. Lee I, Ajay SS, Chen H, Maruyama A, Wang N, McInnis MG (2008) Discriminating single-base difference miRNA expressions using microarray Probe Design Guru (ProDeG). Nucleic Acids Res 36:e27. https://doi.org/10.1093/nar/gkm1165
5. Zhang X, Nie Y, Zhang Q, Liang Z, Wang P, Ma Q (2021) Polydopamine nanoparticles@MoS_2 nanosheet aerogel-based ECL sensing system for MiRNA-126 detection. Chem Eng J 411:128428. https://doi.org/10.1016/j.cej.2021.128428
6. Yang J, Fu S, Luo F, Guo Qiu B, Lin Z (2021) Homogeneous photoelectrochemical biosensor for microRNA based on target-responsive hydrogel coupled with exonuclease III and nicking endonuclease Nb.BbvCI assistant cascaded amplification strategy. Microchim Acta 188:267. https://doi.org/10.1007/s00604-021-04935-6
7. Chu Y, Han T, Deng A, Li L, Zhu JJ (2019) Resonance energy transfer in electrochemiluminescent and photoelectrochemical bioanalysis. Trends Anal Chem 123:115745. https://doi.org/10.1016/j.trac.2019.115745
8. Deng L, Shan Y, Xu JJ, Chen HY (2012) Electrochemiluminescence behaviors of Eu^{3+}-doped CdS nanocrystals film in aqueous solution. Nanoscale 4:831–836. https://doi.org/10.1039/C1NR11470K
9. Zhu W, Saddam Khan M, Cao W, Sun X, Ma H, Zhang Y, Wei Q (2018) Ni$(OH)_2$/NGQDs-based electrochemiluminescence immunosensor for prostate specific antigen detection by coupling resonance energy transfer with Fe_3O_4@MnO_2 composites. Biosens Bioelectron 99:346–352. https://doi.org/10.1016/j.bios.2017.08.005
10. Wang Y, Feng D, Kan X (2022) The combination of highly efficient resonance energy transfer in one nanocomposite and ferrocene-quenching for ultrasensitive electrochemiluminescence bioanalysis. Biosens Bioelectron 210:114347. https://doi.org/10.1016/j.bios.2022.114347
11. Cao JT, Fu YZ, Fu XL, Ren SW (2022) Dual-wavelength electrochemiluminescence ratiometry for hydrogen sulfide detection based on Cd2+-doped g-C3N4 nanosheets. Analyst 147:247–251. https://doi.org/10.1039/d1an01873f
12. Wang XF, Xu JJ, Chen HY (2008) A new electrochemiluminescence emission of Mn^{2+} doped ZnS nanocrystals in aqueous solution. J Phys Chem C 112:17581–17585. https://doi.org/10.1021/jp807136s
13. Ding Z, Quinn BM, Haram SK, Pell LE, Korgel BA, Bard AJ (2002) Electrochemistry andelectrogenerated chemiluminescence from silicon nanocrystal quantum dots. Science 296:1293–1297. https://doi.org/10.1126/science.1069336
14. Chen Y, Zhou S, Li L, Zhu JJ (2017) Nanomaterials-based sensitive electrochemiluminescence biosensing. Nano Today 12:98–115. https://doi.org/10.1016/j.nantod.2016.12.013
15. Du X, Jiang D, Liu Q, Qian J, Mao H, Wang K (2015) Enhanced electrochemiluminescence sensing platform using nitrogen-doped graphene as a novel two-dimensional mat of silver nanoparticles. Talanta 132:146–149. https://doi.org/10.1016/j.talanta.2014.08.065
16. Chaudhari NK, Jin H, Kim B, San Baek D, Joo SH, Lee K (2017) MXene: an emerging two-dimensional material for future energy conversion and storage applications. J Mater Chem A 5:24564–24579. https://doi.org/10.1039/C7TA09094C
17. Naguib M, Mochalin VN, Barsoum MW, Gogotsi Y (2014) 25th anniversary article: MXenes: a new family of two-dimensional materials. Adv Mater 26:992–1005. https://doi.org/10.1002/adma.201304138
18. Osti NC, Naguib M, Ostadhossein A, Xie Y, Kent PR, Dyatkin B, Rother G, Heller WT, Van Duin AC, Gogotsi Y, Mamontov E

(2016) Effect of metal ion intercalation on the structure of MXene and water dynamics on its internal surfaces. ACS Appl Mater Interfaces 8:8859–8863. https://doi.org/10.1021/acsami.6b01490
19. Li X, Yin X, Han M, Song C, Xu H, Hou Z, Zhang L, Cheng L (2017) Ti_3C_2 MXenes modified with in situ grown carbon nanotubes for enhanced electromagnetic wave absorption properties. J Mater Chem C 5:4068–4074. https://doi.org/10.1039/c6tc05226f
20. Chen L, Zeng X, Si P, Chen Y, Chi Y, Kim DH, Chen G (2014) Gold nanoparticle-graphite-like C_3N_4 nanosheet nanohybrids used for electrochemiluminescent immunosensor. Anal Chem 86:4188–4195. https://doi.org/10.1021/ac403635f
21. Seh ZW, Fredrickson KD, Anasori B, Kibsgaard J, Strickler AL, Lukatskaya MR, Gogotsi Y, Jaramillo TF, Vojvodic A (2016) Two-dimensional molybdenum carbide (MXene) as an efficient electrocatalyst for hydrogen evolution. ACS Energy Lett 1:589–594. https://doi.org/10.1021/acsenergylett.6b00247
22. Me A, Kg A, Sv B, Mt A (2012) Structural, optical and magnetic studies on non-aqueous synthesized CdS: Mn nanomaterials-Science Direct. J Alloys Compd 538:48–55. https://doi.org/10.1016/j.jallcom.2012.05.127
23. Rajendran R, Varadharajan K, Jayaraman V, Singaram B, Jeyaram J (2018) Photocatalytic degradation of metronidazole and methylene blue by PVA-assisted Bi_2WO_6-CdS nanocomposite film under visible light irradiation. Appl Nano Sci 8:61–78. https://doi.org/10.1007/s13204-018-0652-9
24. Zhang Q, Teng J, Zou G, Peng Q, Du Q, Jiao T, Xiang J (2016) Efficient phosphate sequestration for water purification by unique sandwich-like MXene/magnetic iron oxide nanocomposites. Nanoscale 13:7085–7093. https://doi.org/10.1039/C5NR09303A
25. Dai H, Wu X, Wang Y, Zhou W, Chen G (2008) An electrochemiluminescent biosensor for vitamin C based on inhibition of luminol electrochemiluminescence on graphite/poly(methylmethacrylate) composite electrode. Electrochim Acta 53:5113–5117. https://doi.org/10.1016/j.electacta.2008.02.044
26. Nie Y, Yuan X, Zhang P, Chai YQ, Yuan R (2019) Versatile and ultrasensitive electrochemiluminescence biosensor for biomarker detection based on nonenzymatic amplification and aptamer-triggered emitter release. Anal Chem 91:3452–3458. https://doi.org/10.1016/10.1021/acs.analchem.8b05001
27. Tavallaie R, McCarroll J, Le Grand M, Ariotti N, Schuhmann W, Bakker E, Tilley RD, Hibbert DB, Kavallaris M, Gooding JJ (2018) Nucleic acid hybridization on an electrically reconfigurable network of gold-coated magnetic nanoparticles enables microRNA detection in blood. Nat Nanotechnol 11:1066–1071. https://doi.org/10.1038/s41565-018-0232-x
28. Shi CX, Li YZ, Liu Q, Chen ZP, Li SS, Yu RQ (2021) Label-free microRNA detection through analyzing the length distribution pattern of the residual fragments of probe DNA produced during exonuclease III assisted signal amplification by mass spectrometry. Talanta 231:122414. https://doi.org/10.1016/j.talanta.2021.122414
29. Li M, Xu X, Cai Q (2021) DNA polymerase/NEase-assisted signal amplification coupled with silver nanoclusters for simultaneous detection of multiple microRNAs and molecular logic operations. Sensors Actuators B Chem 327:128915. https://doi.org/10.1016/j.snb.2020.128915
30. Cheng X, Ren D, Xu G, Wei F, Yang J, Xu J, Wang L, Hu Q, Cen Y (2021) Metal-organic frameworks-assisted nonenzymatic cascade amplification multiplexed strategy for sensing acute myocardial infarction related microRNAs. Biosens Bioelectron 196:113706. https://doi.org/10.1016/j.bios.2021.113706
31. Ying ZM, Tu B, Liu L, Tang H, Tang LJ, Jiang JH (2018) Spinach-based fluorescent light-up biosensors for multiplexed and label-free detection of microRNAs. Chem Commun 24:3010–3013. https://doi.org/10.1039/C8CC00123E
32. Slabý J, Bocková M, Homola J (2021) Plasmonic biosensor based on a gold nanostripe array for detection of microRNA related to myelodysplastic syndromes. Sensors Actuators B Chem 347:130629. https://doi.org/10.1016/j.snb.2021.130629
33. Tu W, Cao H, Zhang L, Bao J, Liu X, Dai Z (2016) Dual signal amplification using gold nanoparticles-enhanced zinc selenide nanoflakes and P19 protein for ultrasensitive photoelectrochemical biosensing of microRNA in cell. Anal Chem 88:10459–10465. https://doi.org/10.1021/acs.analchem.6b02381